LAWRENCE
LIVERMORE
NATIONAL
LABORATORY

LLNL-JRNL-623392

Low density biodegradable shape memory polyurethane foams for embolic biomedical applications

P. Singhal, W. Small, E. Cosgriff-Hernandez, D. Maitland, T. Wilson

February 28, 2013

Acta Biomaterialia

Disclaimer

Low density biodegradable shape memory polyurethane foams for embolic biomedical applications

Pooja Singhal[1,2], Ward Small[1], Elizabeth Cosgriff-Hernandez [2], Duncan J Maitland*[2],Thomas S Wilson*[1]

Affiliations

[1] 7000 East Avenue, Lawrence Livermore National Laboratory, Livermore, CA 94550 USA

[2] 5045 Emerging Technologies Building, Department of Biomedical Engineering, 3120 Texas A&M University, College Station, TX 77843-3120 USA

Corresponding Authors:

Dr. Duncan J. Maitland

Department of Biomedical Engineering, 5057 Emerging Technologies Building,

3120 Texas A&M University, College Station, TX 77843-3120 USA.

Email: djmaitland@tamu.edu; Phone: 979-458-3471; Fax: 979-845-4450

Dr. Thomas S. Wilson

Physical and Life Sciences Directorate, 7000 East Avenue,

Lawrence Livermore National Laboratory, Livermore, CA 94550 USA

Email: wilson97@llnl.gov

Abstract

Low density shape memory polymer foams hold significant interest in the biomaterials community for their potential use in minimally invasive embolic biomedical applications. The unique shape memory behavior of these foams allows them to be compressed to a miniaturized form, which can be delivered to an anatomical site via a transcatheter process, and thereafter actuated to embolize the desired area. Previous work in this field has described the use of a highly covalently crosslinked polymer structure for maintaining excellent mechanical and shape memory properties at the application-specific ultra low densities. This work is aimed at further expanding the utility of these biomaterials, as implantable low density shape memory polymer foams, by introducing controlled biodegradability. A highly covalently crosslinked network structure was maintained by use of low molecular weight, symmetrical and polyfunctional hydroxyl monomers such as Polycaprolactone triol (PCL-t, M_n 900 g), N,N,N_0,N_0-Tetrakis (hydroxypropyl) ethylenediamine (HPED), and Tris (2-hydroxyethyl) amine (TEA). A control over the degradation rate of the materials was achieved by changing the concentration of the degradable PCL-t monomer, and by varying the material hydrophobicity. These low density porous SMP materials demonstrated a uniform cell morphology and excellent shape recovery, along with controllable actuation temperature and degradation rate. We believe that they form a new class of low density biodegradable SMP scaffolds that can potentially be used as "smart" non-permanent implants in multiple minimally invasive biomedical applications.

Keywords: Shape Memory Polyurethane, Polycaprolactone triol, low density foams, degradation rate, FTIR.

1. Introduction

Approximately 25,000-30,000 people suffer from death or severe debilitation as a result of Sub-Arachnoid Hemorrhage (SAH) from aneurysm rupture in the US per year.[1] Rupture of small and large necked aneurysms constitutes nearly 40% and 50% of these SAHs, respectively. However, the currently available endovascular technique for the treatment of aneurysms, using Guglielmi Detachable Coils (GDCs), is successful in completely occluding only ~85% of small necked aneurysms and ~15% of large necked aneurysms.[2] In addition, the GDC procedure has other drawbacks, such as, requiring delivery of multiple coils with a 1.4 - 2.7% chance of rupture of the aneurysm with every delivered coil [1], post-operative coil compaction [3], and shifting or even migration of the coils out of the aneurysm [4] causing risks of aneurysm re-growth or rupture/stroke. In face of these risks, there is a persistent need for an improved endovascular treatment of intracranial aneurysms.

Shape Memory Polymer (SMP) foam based devices are being actively investigated as an improved endovascular alternative to the GDCs.[5, 6] Several materials including polyurethane and epoxy based SMP foams have been investigated for a wide range of applications utilizing their unique ability of "smart" shape recovery on actuation, [7-12] and a comprehensive review of literature on porous SMPs has recently been published [13]. However, embolic medical applications, such as aneurysm treatment, require some critical material properties. Most importantly, materials with ultra low densities, thereby enabling transcatheter delivery and high volume expansion on actuation, are required. In addition, they should maintain good mechanical properties and excellent shape recovery despite the ultra low densities. To achieve these objectives, a new class of highly covalently crosslinked SMP foams was developed by our group

[14] based on the materials proposed by Wilson et al. [15] Extensive investigation of these materials has been done in recent years. Studies critical to their embolic application in treatment of aneurysms, such as of their mechanical properties and shape memory behavior [14], inclusion of contrast agent for enabling *in vivo* imaging during device delivery [16], stresses experienced on the aneurysm wall during actuation/implantation [17], effect of moisture on the foam's actuation temperature, [18] variation in composition to control the rate of actuation of foams in presence of moisture [19], and *in vivo* implantation in porcine models [20] have been performed. Based on the promising outlook of these materials as reported in these studies, it was further desirable to make them biodegradable. It was hypothesized that if the implant degraded over time after the initial endothelialization of the aneurysm neck, the isolated aneurysmal bulge would eventually atrophy leading to a complete cure of the vasculature.

In order to achieve biodegradability, we developed a series of low density foams using Polycaprolactone Triol (PCL-t, M_n 900 g). PCL-t was a monomer of choice for introducing hydrolytically degradable ester linkages in these materials, both because it is a trifunctional monomer, in agreement with the desired highly covalently crosslinked network structure [14], and because Polycaprolactone (PCL) is an FDA approved polymer that is extensively used in tissue engineering applications such as the regeneration of bone [21], ligament [22], skin [23, 24], nerve [25, 26], and vascular tissues [27]. Although a relatively low rate of degradation (2-3 years) has been observed in PCL based materials due to its high crystallinity, this degradation rate is tunable and has been shown to increase with decreasing crystallinity. [28]

Here we report the synthesis process of these covalently crosslinked and amorphous degradable

SMP foams based on PCL-t, N,N,N_0,N_0-Tetrakis (hydroxypropyl) ethylenediamine (HPED), Tris (2-hydroxyethyl) amine (TEA), and water as the hydroxyl monomers. Control over the rate of degradation is attempted by a) changing the concentration of the degradable PCL-t monomer, and b) introducing isocyanates of higher hydrophobicity, namely Trimethyl hexamethylene diisocyanate (TMHDI) and Isophorone diisocyanate (IPDI), in addition to Hexamethylene diisocyanate (HDI). Increase in the hydrophobicity of the monomers was of interest not only for its effect on the rate of degradation, but also for limiting the rate of plasticization of the polymer in physiological media, in order to enable transcatheter delivery of the device. [19] Characterization of density, cell structure, thermochemical properties, shape memory, and the degradation mechanism and rate of the foams are reported, and discussed with respect to an ideal device for aneurysm treatment.

2. Materials and Methods

2.1 Synthesis of foams

Foam compositions are given in **Table 1**. All chemicals, PCL-t (M_n 900 g, Sigma Aldrich Inc.), HPED (99%, Sigma Aldrich Inc.), TEA (98%, Alfa Aesar Inc.), HDI (TCI America Inc.), TMHDI (TCI America Inc.), IPDI (TCI America Inc.), and DI water (>17 M**Ω**-cm purity, Millipore) were used as received. Foams were synthesized in a three-step method as previously reported. [14] Inclusion of the ester bonds in polymer composition however required significant optimization of the type and amount of surfactants and catalysts for viable foams, relative to previously reported formulations. Optimized levels of amine based catalyst (BL-22, Air Products Corp.), tin based catalyst (T-131, Air Products Corp.) and silicone based surfactants (DCI990 and DC5179, Air Products Corp.) as used for foam synthesis, are reported in Table 1. Foam

compositions 100P-HDI, 50P-HDI, 25P-HDI and 0P-HDI refer to formulations with 100%, 50%, 25% and 0% (control) of hydroxyl equivalents from PCL-t, and the remaining from HPED and TEA in a 2:1 ratio. This denomination excludes the 41% of isocyanate equivalents that are consumed in reaction with water (chemical blowing agent), while maintaining a 104 isocyanate index in the net foam formulation. The foam compositions 100P-TMHDI and 100P-IPDI refer to formulations where HDI is completely replaced with TMHDI and IPDI respectively in the 100P-HDI foams (Table 1).

2.2 Density and cell structure

Core density of the foam was measured from the representative top and middle sections of the foam as per the ASTM standard D-3574-08. Average values over 5 samples are reported for each composition. Cell structure was characterized using a low vacuum scanning electron microscope (NeoScope JCM 5000, Nikon). Foam samples were mounted on the stage and their surface morphology was captured at 5 kV accelerating voltage and 50X magnification.

2.3 Differential Scanning Calorimetry (DSC)

Glass transition temperature (T_g) was measured using a Pyris Diamond DSC (PerkinElmer Inc.). A 3-5 mg sample was loaded in a vented aluminum pan at room temperature, cooled to -60 °C and then run through a heat - cool - heat cycle from -60 to 120 °C at a rate of 20 °C min^{-1}. The half-height of the transition during the second heat was taken as an estimate of the T_g.

2.4 Fourier Transform Infrared (FTIR) Spectroscopy

An FTIR spectrum of the foams was collected using a Spectrum 2000 FTIR (Perkin Elmer Inc.). The sample chamber was purged with nitrogen gas for 5 minutes and a background spectrum was captured. Thereafter, thin slices (~2-4 mm in thickness) cut from foam blocks were placed in a 2 cm^{-1} JStop holder (0.88 cm aperture). The chamber was again purged with nitrogen for 5 minutes after placing the sample, and an FTIR spectrum was collected in the absorption mode at a resolution of 4 cm^{-1}. The test was performed in duplicate to ascertain reproducibility of the spectra. A total of 50 scans were taken for each sample and the background spectrum was subtracted using the Spectrum software (Perkin Elmer Inc.). Also, a baseline correction was performed on the resulting spectra to account for the scattering of the IR beam across the sample.

2.5 Shape memory behavior

To quantify the shape memory behavior, constrained stress recovery tests were performed in compressive mode using the parallel plate fixture in a ARES-LS2 rheometer (TA Instruments Inc.). Cylindrical samples of 100P-HDI foam (~20 mm diameter and ~15 mm height) were tested (T_g ~ -20 ^oC). The sample was first heated up to a temperature of T_g+40 ^oC (20 ^oC) and deformed to a 60% compressive strain at a rate of 2.5 mm min^{-1} (loading). Thereafter, the sample was cooled to T_g-30 ^oC (-50 ^oC) (fixing), followed by heating back up to T_g+40 ^oC (stress recovery) while mantaining the 60% strain. At the end of the cool-heat cycle, the strain was released at a rate of 2.5 mm min^{-1} (unloading), and the recovered strain was obtained from the distance between the plates when the axial force dropped to 5 g. The sample stress was monitored throughout the loading-fixing-stress recovery-unloading cycle, and five consecutive cycles were performed. Also, the final recovered sample height post cyclic testing was measured after a

relaxation period of 24 hours at T_g+40 ^{o}C (20 ^{o}C) to estimate the time dependence of the shape recovery. A total of five samples were tested for shape memory behavior.

2.6 Degradation behavior

For testing the degradation behavior of the materials, degradation in both alkaline medium (0.1 N NaOH, accelerated degradation) and phosphate buffer saline medium (PBS, physiological degradation) were performed. Rectangular (1 cm by 2 cm) strips of foam 2-4 mm in thickness were cut from the representative areas of the foam stock. The foam samples were cleaned using a previously reported protocol for removal of residual foaming additives and partial rupture of cell membranes.[19] Briefly, the samples were soaked in 0.1 N HCl solution under sonication for 2 hours, and then cleaned for two 15 minute cycles each with a) 80-20 volume% solution of DI water and Conrad 70, and b) DI water, under sonication. Thereafter, the cleaned foams were dried under vacuum at 50 ^{o}C overnight.

The degradation study was conducted for a period of 7 months with analysis of mass loss and changes in the physical and chemical structures of the materials conducted weekly for the first 3 months, followed by once every ~3 weeks. First, the initial weight, FTIR, and gross morphology of the samples were recorded. Thereafter, they were placed in a ~1000 times weight excess of the media in labeled vials at 37 ^{o}C. Vacuum was pulled on the submerged samples overnight (~12 hours) for removal of air bubbles that may otherwise inhibit the contact of media with the polymer. Following this period the vacuum was released, and the vials were refilled to account for any loss in media due to vacuum. It was ensured that all the samples were completely submerged in water and were void of any air bubbles. Samples remained in the oven at 37 ^{o}C for

the next 6 days to undergo degradation. After this degradation period, the media was removed and the samples were rinsed in DI water, followed by drying under vacuum at 50 ^{o}C overnight. Characterization of the dried samples was performed prior to repeating their submersion in the degradation media.

2.6.1 Mass loss

For estimating the pattern of mass loss of the polymers, ten samples of each composition and each media type were tested. An Ohaus Analytical Plus scale (AP250D, Central Carolina Scale Inc.) with a resolution of 0.01 mg was used for the weight measurements. Mass of samples was recorded initially (W_i), and after every week (n) of degradation (Wn). The % degradation at the n^{th} week was calculated as:

$$\%\ mass\ loss = \frac{W_i - W_n}{W_i} \times 100\ ;n = 1\ to\ 28$$

The average % mass loss and standard deviation, calculated over the 10 samples, were reported.

2.6.2 FTIR

Foam FTIR spectra were collected using a Spectrum 2000 FTIR (Perkin Elmer Inc.) according to the procedure detailed above (Section 2.4). Spectral changes were monitored as a function of degradation time with particular attention given to ester, urethane, and urea absorbance bands. The spectra were normalized with respect to the alkyl absorbance at 2857 cm^{-1} for analysis. However, as the alkyl groups may not remain conserved throughout the degradation period for all compositions, only a qualitative analysis of the shift in peak absorbance was performed to estimate the mechanism of degradation.

2.6.3 Gross morphology

Changes in the gross morphology of the foams, as a function of the degradation time, were captured using a camera (SX230HS, Canon Inc.). An analysis of visible morphological changes due to the sample degradation was performed from the images.

3. Results

3.1 Density and cell structure

Density values of different foam compositions are reported in **Table 2**. Foam densities ranging from 0.020 to 0.093 g cm^{-3} were recorded. These values correspond to an average porosity of greater than 90% for all compositions $\% \, porosity = \ \rho_{neat} - \rho_{porous} \ \times 100 \ \rho_{neat}$; here ρ_{porous} is the foam density and average ρ_{neat}~1.1 g cm^{-3} is the neat/unfoamed polymer density. The relatively small standard deviation (0.002 - 0.015 g cm^{-3}) in densities indicates good uniformity of the individual foam samples.

Cell structure of the foams is shown in **Figure 1**. A closed, or mixed closed to open, cell structure was observed for all foams. Thin residual membranes, similar to those reported for related materials previously [14, 19], were seen on the cell surfaces. Overall, the images depicted a high level of uniformity in the cell structure of a given foam composition. This is largely attributed to the use of the gas blowing process for foam fabrication, as well as optimization of the foaming additives and process parameters. For instance, fabrication of related polyurethane foams from PCL-t and HDI using the High Internal Phase Emulsion (HIPE) templating process by David et al. produced comparatively higher densities (0.21 g cm^{-3}), with large variation in

pore size ranging from ~1 mm (from the CO_2 bubbles during reaction of isocyanate with water) to ~ 0.1-100 um.[29]

3.2 DSC

Glass transition temperature (T_g) values of different foam compositions are reported in Table 2 and **Figure 2**. The T_g of foams was seen to decrease with increase in the PCL-t content from 70 ^oC (0P-HDI) to -19 ^oC (100P-HDI). This is expected as the trifunctional PCL-t molecule can increase the free volume in the amorphous polymer network due to its longer branches relative to HPED and TEA. This increase in free volume can consequently increase the mobility of the polymer chains, and reduce the polymer T_g. Also, replacing the HDI in the 100P-HDI composition with TMHDI and IPDI was seen to increase the T_g of the foams. TMHDI is expected to increase the T_g of the foams, relative to HDI, as the methyl groups of TMHDI can increase the energy required by the molecule to rotate about the backbone bonds. However, its effect was relatively small (~8 ^oC). IPDI was seen to increase the foam T_g relative to HDI by a much larger extent of ~45 ^oC. This may be attributed to the significant increase in the stiffness of the backbone due to the presence of the saturated ring of IPDI in the isocyanate molecule. It is noteworthy that a single glass transition was seen for all materials. Absence of any secondary transition indicates an amorphous network structure, and formation of an all-encompassing crosslinked network with no isolated pockets of unreacted monomer that were reported for related compositions by David et al.[29]

3.3 FTIR

FTIR spectra of foams are shown in **Figure 3** and **4,** and labeled to highlight peaks corresponding to ester, urethane and alkyl groups that were utilized in the degradation analysis. The urethane carbonyl band was observed in the range of 1695-1700 cm^{-1} for all compositions.[30] It is clearly visible in the 0P-HDI through 50P-HDI compositions; however, it was masked by the ester peak in the 100P-HDI, 100P-TMHDI and 100P-IPDI compositions. The urethane δ(N-H) + ν(C-N) amide II and amide III bond absorbance were observed at 1530-1540 cm^{-1} and 1235-1250 cm^{-1}, respectively. A urea shoulder from reaction of isocyanate with water (chemical blowing agent) was observed at ~1630-1650 cm^{-1} for all compositions.[30] The ester carbonyl absorbance at 1730 cm^{-1} increased with increasing PCL-t content relative to the urethane carbonyl.[30] Similarly the ester asymmetric ν(C-O-C) absorbance at 1236 cm^{-1} and the symmetric ν(C-O-C) ester absorbance at 1160 cm^{-1} also increased with increasing PCL-t content.[30] The changes in the spectra from CH_3 groups of TMHDI and saturated ring of IPDI were seen in the 2800-3000 cm^{-1} range in the 100P-TMHDI and 100P-IPDI compositions, respectively. [30]

The trends of relative FTIR absorbance were as expected. Increase in the PCL-t content of the foam (0P/25P/50P/100P-HDI) results in an increased ester content of the material. This was adequately reflected in the successive increase of ester carbonyl (C=O), and the asymmetric and symmetric ester ether (ν(C-O-C)) band absorbance in these compositions. Further, as the compositions with different isocyanate type (100P- HDI/TMHDI/IPDI) exclusively used PCL-t as the hydroxyl monomer, no difference in the relative ester and urethane absorbance was observed within these compositions; however, expected variation in the signature isocyanate fingerprints could be identified in the alkyl absorbance band.

3.4 Shape memory behavior

Shape memory behavior of the 100P-HDI foam samples is reported in **Figure 5**. The results obtained were similar to those obtained in a previous study of related compositions [14], i.e. the shape recovery was relatively lower for initial cycles and was seen to improve for successive cycles. An average shape recovery of 91±3%, 94±1%, 96±1%, 98±1%, and 99±1% respectively was recorded for the five consecutive cycles over five samples. The loss in shape recovery in the initial few cycles is often attributed to macroscopic changes in the material, such as damage to cell struts/membranes [14]. However, on storage at $T > T_g$ (20 ^oC) for ~24 hours after the cyclic testing, the samples showed a consistent recovery to 98-99% of their original dimensions. Hence a significant part of the otherwise minor loss in recovery in the initial cycles was eventually recovered.

3.5 Degradation behavior

3.5.1 Mass loss

The mass loss profile of the various foam compositions in 0.1 N NaOH is presented in **Figure 6**. Both reducing the PCL-t content, and increasing the hydrophobicity of the isocyanate monomer, were seen to significantly reduce the rate of mass loss. The 100P-HDI composition was observed to have the highest mass loss rate. It underwent rapid degradation, and the sample was irretrievable post week 6. Fragments of the disintegrated polymer could be seen in the degradation media at week 7. These fragments gradually decreased in size and eventually reached the critical chain length for aqueous solubility, thereby undergoing complete dissolution in the media. The 100P-TMHDI sample demonstrated a relatively slower mass loss, and the

sample did not disintegrate completely until week 15. But eventually complete dissolution of the polymer fragments was observed in the media, similar to those of the 100P-HDI composition. 100P-IPDI showed a still slower degradation rate, and maintained its structural integrity through the entire test duration of 7 months. The increase in material hydrophobicity with use of TMHDI and IPDI is expected to be responsible for the reduced mass loss rate in these compositions.

The rate of mass loss for both 50P-HDI and 25P-HDI compositions was also successively lower relative to that of 100P-HDI, and they did not disintegrate during the test period. This rate is expected to be limited by the diffusion of the degraded molecular fragments from the polymer. As the content of PCL-t was lower in these compositions, the average molecule size diffusing out is expected to be larger, leading to a lower rate of mass loss. Also, with a lower concentration of degradable linkages, the probability for all the branches of these crosslinked materials to get lysed and be eroded from the network is expected to decrease, again lowering the rate of mass loss. No significant mass loss was noticed for the 0P-HDI in 0.1 N NaOH, or for any composition in the PBS media during the 7 month test period.

3.5.2 FTIR

FTIR spectra for various compositions during the first 12 weeks of degradation are shown in **Figure 7**. The 100P-HDI composition (Figure 7) registered a small decrease in the absorbance of ester carbonyl at 1730 cm^{-1} in the first week. This absorbance was further reduced in the 2^{nd} week of degradation, and was negligible by the 3^{rd} week. Concomitant reduction in the urethane carbonyl at 1395-1370 cm^{-1} was also observed. Hydrolysis of the urethane bond is likely not the primary cause of this reduction given that the adjacent ester bonds are more susceptible to

hydrolysis. Therefore, this loss of absorbance was attributed to solubilization of low molecular weight polymer segments containing urethane linkages after hydrolysis of the adjacent ester. The rapid mass loss prevented collection of FTIR spectra after week 4, and the sample was irretrievable post week 6. The FTIR spectra of the 100P-TMHDI composition followed the same pattern as that of 100P-HDI (Figure 7), but the rate of degradation was slower. No significant change was noticed in the spectrum despite the mass loss until week 5. This suggests the dominance of surface degradation during the initial 5 weeks. Specimens incubated for 6 weeks displayed a loss of absorbance of ester carbonyl at 1730 cm^{-1}, indicative of initiation of bulk degradation at this stage. The sample was finally irretrievable at week 15. No significant variation was observed in the FTIR spectra of 100P-IPDI during the 12 weeks (Figure 7), despite the fixed pattern of mass loss. This may again indicate presence of primarily a surface degradation mechanism, rather than bulk erosion. The transition from bulk erosion in 100P-HDI to the primarily surface degradation mechanism of 100P-TMHDI and 100)-IPDI was attributed to the increased hydrophobicity of these polymers as compared to HDI. This increase in hydrophobicity limits access of the aqueous degradation media to the ester linkages in the bulk of the sample.

FTIR spectra of the 50P-HDI are also shown in Figure 7. Similar to the 100P-HDI spectra, a decrease in the ester absorbance at 1730 cm^{-1} is observed, indicating attack of the media throughout the entire bulk of the material. However, a relatively lower rate of decrease in ester absorbance is noticed, compared to that of 100P-HDI. Also, an increase in the absorbance of urea (~1620-1650 cm^{-1}) was noticed over time, indicating the relative decrease in the absorbance of urethane bond. A similar degradation pattern was again observed in 25P-HDI composition

(Figure 7) with a still lower rate of decrease in ester absorbance. The trend of decrease in the ester absorbance of these compositions is in agreement with the pattern of mass loss, and the decreasing content of PCL-t monomer containing the hydrolysable ester groups. Finally, no statistically significant change in the FTIR spectra was noticed for the 0P-HDI composition (control) throughout the degradation period, which is again in agreement with its negligible mass loss.

3.5.3 Gross morphology

Gross morphology of the fastest degrading 100P-HDI composition at the weekly time points is shown in **Figure 8**. The sample did not develop cracks or fracture lines during the test period. The material degradation was relatively uniform throughout the sample and may be attributed to the completely amorphous polymer structure, high hydrophilicity, and the morphological properties of low density and uniform cell structure. This indicates a bulk degradation mechanism for this composition, in agreement with the FTIR results.

4. Discussion

Several biodegradable SMPs have been reported in the literature.[31] A recent review by Behl et. al. reports biodegradable SMPs developed in the four primary SMP network structure categories of covalently crosslinked crystalline and amorphous networks, and physically crosslinked crystalline and amorphous networks.[31] Multiple PCL based physically and covalently crosslinked crystalline biodegradable polymers have also been reported.[31] Particularly, covalently crosslinked amorphous biodegradable SMP networks, as proposed in this work, have been reported from coupling star-shaped hydroxyl- telechelic polyesters with a diisocyanate.[32]

In this polymeric system, star shaped precursors were developed from reaction of polyfunctional initiators such as 1, 1, 1 - tris(hydroxymethyl)ethane, and pentaerythrite with copolyester segments from diglycolide or other cyclic diesters, and dilactide. Incorporation of a second immiscible phase, such as poly(propylene glycol), in varying content and molecular weight allowed precise control over the mechanical properties of this family of polymers. Another covalently crosslinked amorphous polymeric system was derived from UV polymerization of poly[(l-lactide)-ran-glycolide] dimethaycrylates (PLGDMA), which in turn were obtained from methacryloyl chloride based functionalization of hydroxy telechelic poly[(l-lactide)-ran-glycolide] (PLG) ($1000 < M_n < 5700$ g mol^{-1}).[33] Also, a photo crosslinked linear ABA triblock precursor poly(rac-lactide)-b-poly(propylene oxide)-b-poly(rac-lactide) dimethacrylate was reported, where M_w of rac-lactide was varied from 2000 to 6000 g mol^{-1} in conjunction with a 4000 g mol^{-1} block of polypropylene glycol to control the mechanical properties of the material.[34] Of these materials, the polyurethanes from the star-shaped hydroxyl-telechelic polyesters of M_w ~870-1000 have a polymer architecture closest to that of the materials reported here, but these were developed in their neat/non-porous form.

To our knowledge, there is limited availability of amorphous biodegradable SMPs that simultaneously show a polymer architecture comprising high density of covalent crosslinks, and a low density porous morphology, as desired for embolic applications.[14] Related compositions of PCL-t (900 g) with HDI have been reported by David et al. using the HIPE process; however, the foams were relatively dense with a non-uniform cell structure.[29] The use of the gas blowing process for these compositions, as reported here, not only enabled reasonably low densities (0.020-0.093 g cm^{-3}), but also gave a very uniform cell morphology. In part, this is a

result of optimization of the DCI990 and DC5179 surfactants to better stabilize the foam structure in the presence of the relatively high molecular weight PCL-t (900 g). Also the viscosity of the foaming solution was adjusted across different compositions by changing the OH/NCO ratio of the isocyanate premix to assist in the foam rise. Additional optimization of the foaming solution viscosity and the type and level of the surfactants and additives during the foaming process [14], may however still be conducted to further control the foam porosity/density and cell structure while maintaining the shape memory properties.

Degradation rate of the materials was observed to be lower for lower PCL-t content, as well as for more hydrophobic, 100P-TMHDI and 100P-IPDI, compositions. A large portion of the synthetic biomaterials used in resorbable devices utilize hydrolytically labile groups to impart a biodegradable character. The primary steps in the hydrolytic degradation process, employed by these materials, have been identified as a) diffusion of the water in the polymer matrix, b) cleavage of the bonds susceptible to hydrolysis, resulting in low molecular weight chains or oligomers, and c) diffusion of these cleaved chains out of the polymer resulting in mass loss.[35] Consequently, the rate of mass loss or degradation can be altered by: 1) water uptake, which is influenced by the polymer composition; or 2) the rate of hydrolysis, which is influenced by the type of chemical bond and the degradation media. It is expected that the use of more hydrophobic TMHDI and IPDI monomers would decrease the water uptake of the polymers relative to HDI, thereby affecting the rate of cleavage of hydrolytic ester bonds. Indeed, surface degradation, as opposed to bulk degradation, was observed to be more dominant in the materials as the hydrophobicity was increased. Use of a lower amount of PCL-t content made it slower for a cleaved oligomer to readily diffuse out, again leading to a lower rate of mass loss. However,

these materials showed a more bulk degradation effect due to their relatively hydrophilic nature from the use of HDI. This degradation study was accelerated via use of a pH 13 media (0.1 M NaOH solution), in order to achieve measurable rates in shorter time frames. No statistically significant mass loss was recorded for samples in the physiological PBS degradation media over the duration of this study. But as crystalline PCL has been shown to undergo degradation in 2-3 years in a physiological medium [28], it is expected that the 100P-HDI composition would degrade earlier than that due to its amorphous state. *In vivo* implantation of these materials will be subject to enzymatic degradation as well, which may further increase the degradation rate. Further, the aliphatic monomers used in these compositions are expected to release biocompatible degradation products. However, animal studies or cell culture tests will need to be performed to fully ascertain the material biocompatibility.

A decrease in the T_g of the material was observed with a decrease in hydrophobicity and increase in the PCL-t content. For polyurethane materials, the as-measured dry T_g has been reported to get further depressed on exposure to water/physiological media [19]. Hence, for use of these materials for intravascular aneurysm embolization, it is essential that the depressed/plasticized T_g in fluid media is above body temperature (37 ºC) to prevent premature actuation of the device during transcatheter delivery. Based on the trends observed here, a T_g of 35-40 ºC may be achieved by substituting part of PCL-t with HPED or TEA in the 100P-IPDI composition, while still maintaining degradability of the material. As IPDI is relatively hydrophobic, further depression in T_g in presence of water/physiological media may also not be as significant, facilitating the *in vivo* transcatheter delivery of the device.[19] It is noteworthy though, that because the rate of degradation of materials is directly affected by the uptake of water, it may not

be possible to achieve a material with a high degradation rate, as well as a low degree of plasticization, in water/physiological media. Hence, it is suggested that a different strategy, such as surface modification, may be employed to limit the plasticization rate during delivery of the device made from an otherwise hydrophilic/faster degrading material.

5. Conclusion

A series of novel biodegradable shape memory polymer foams were synthesized for embolic biomedical applications, particularly the transcatheter treatment of aneurysms. Following is a summary of key results:

1) A highly covalently crosslinked polymer network structure was developed by use of the degradable trifunctional monomer PCL-t (M_n 900 g), and the tri- and tetra- functional monomers TEA and HPED, respectively, to ensure excellent shape memory behavior at the very low densities of 0.020 – 0.093 g cm^{-3}.
2) A uniform cell structure was observed across all compositions, and a high shape recovery (~98-99%) was recorded for the 100P-HDI foams. Given their similar network structure, all other compositions are also expected to exhibit excellent shape recovery.
3) The T_g was observed to decrease with an increase in the content of the degradable monomer PCL-t. Also, an increase in the T_g was recorded with the increase in the hydrophobicity of the material via incorporation of more hydrophobic monomers, TMHDI and IPDI, in lieu of HDI. A controlled T_g variation from -19 ºC to 29 ºC was thereby achieved.
4) The degradation rate was found to be dependent on the PCL-t content, as well as the hydrophobicity of the composition. The composition with the highest PCL-t content and

lowest hydrophobicity (100P-HDI) achieved complete degradation in 0.1 N NaOH in 5 weeks. On the other hand, replacing the HDI with more hydrophobic monomers or reducing the PCL-t content, greatly reduced the degradation rate with 100P-IPDI and 25P-HDI showing only ~29% and 25% mass loss respectively at 28 weeks. Further, surface degradation mechanism was observed to be more prominent for materials with higher hydrophobicity (100P-TMHDI and 100P-IPDI).

The excellent morphological and shape memory properties, in conjunction with the control over the degradation rate of these biodegradable foams, classify them as an important class of low density smart scaffolds for biomedical applications, especially those involving minimally invasive transcatheter surgery.

6. Acknowledgement

This work was partially performed under the auspices of the U.S. Department of Energy by Lawrence Livermore National Laboratory (LLNL) under Contract DE-AC52-07NA27344 and supported by the National Institutes of Health/National Institute of Biomedical Imaging and Bioengineering Grant R01EB000462 and by Lawrence Livermore National Laboratory Directed Research and Development (LDRD) Grants 04-LW-054 and 04-ERD-093. The authors thank Dr. Steve Letts, Dr. Michael Stadderman, and Dr. Suhas Bhandarkar at LLNL for their assistance with the FTIR experiments.

7. Figures and Tables

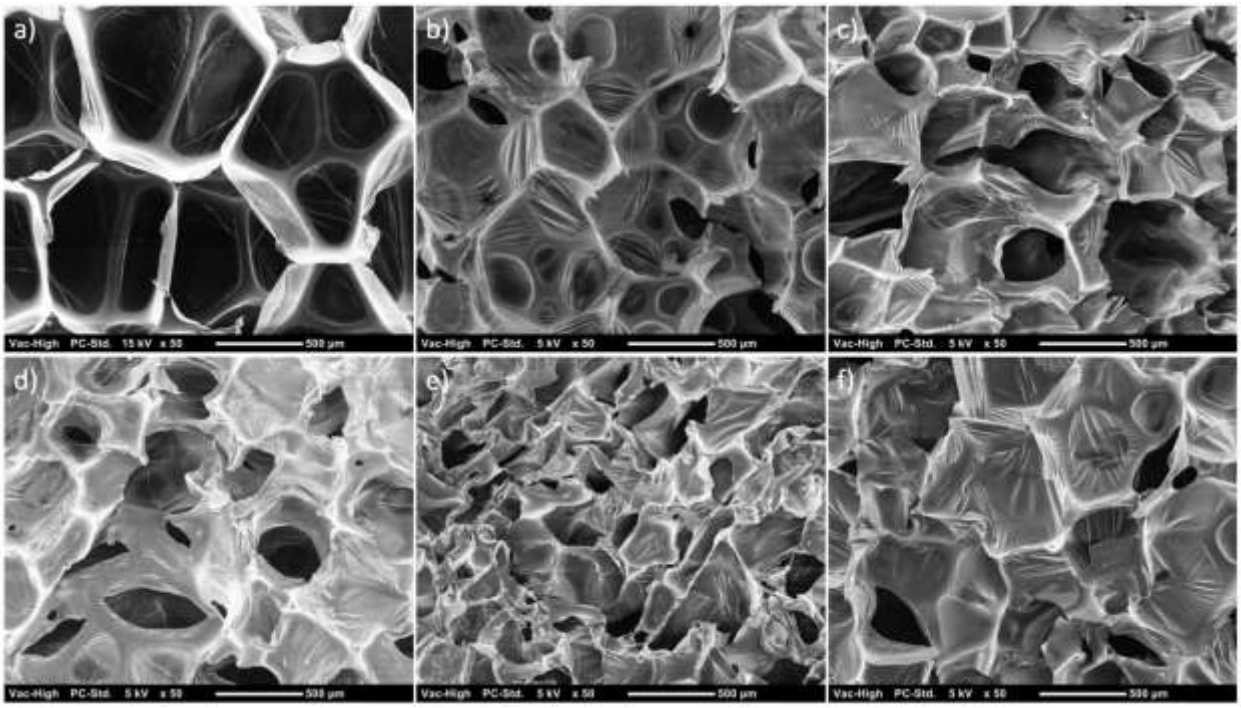

Figure 1. Cell structure as seen from Scanning Electron Microscopy for a) 0P-HDI, b) 25P-HDI, c) 50P-HDI, d) 100P-HDI, e) 100P-TMHDI, and f) 100P-IPDI foam compositions. A mixed open to closed cell morphology, with uniform cell structure is observed for all compositions. Scale bar=500 um.

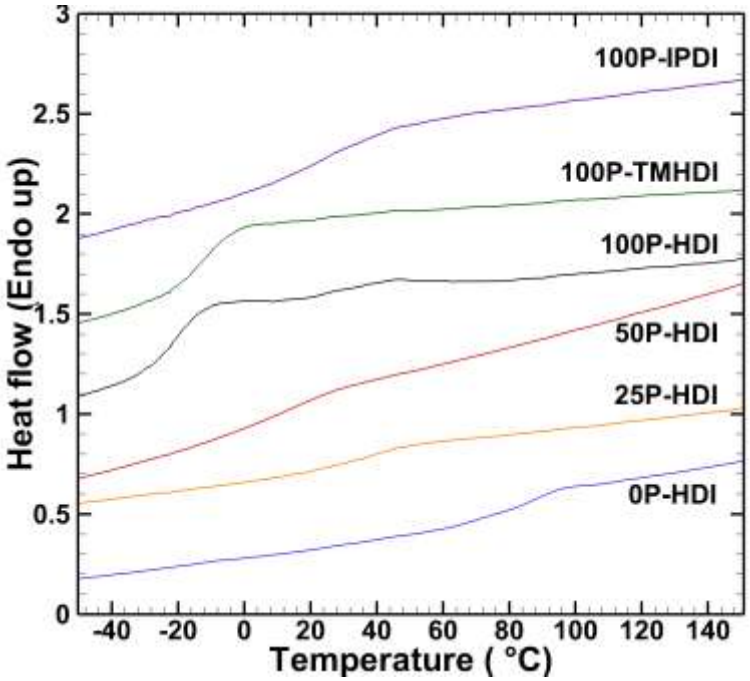

Figure 2. Differential scanning calorimety (DSC) curves of various foam compositions show a single T_g indicating an amorphous polymer network structure.

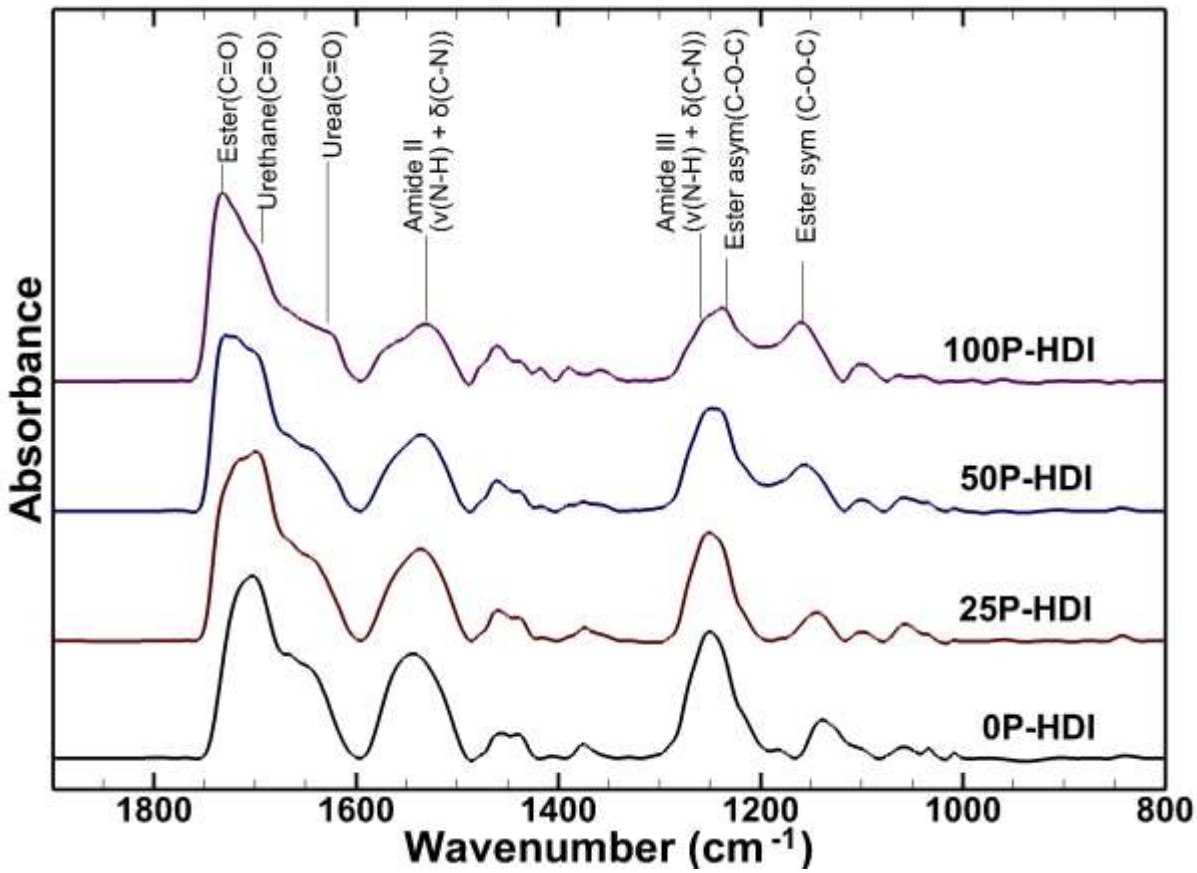

Figure 3. FTIR spectra of the samples with varying PCL-t content prior to degradation. Peaks corresponding to the ester, urethane and urea bonds are labeled for identification of respective trends.

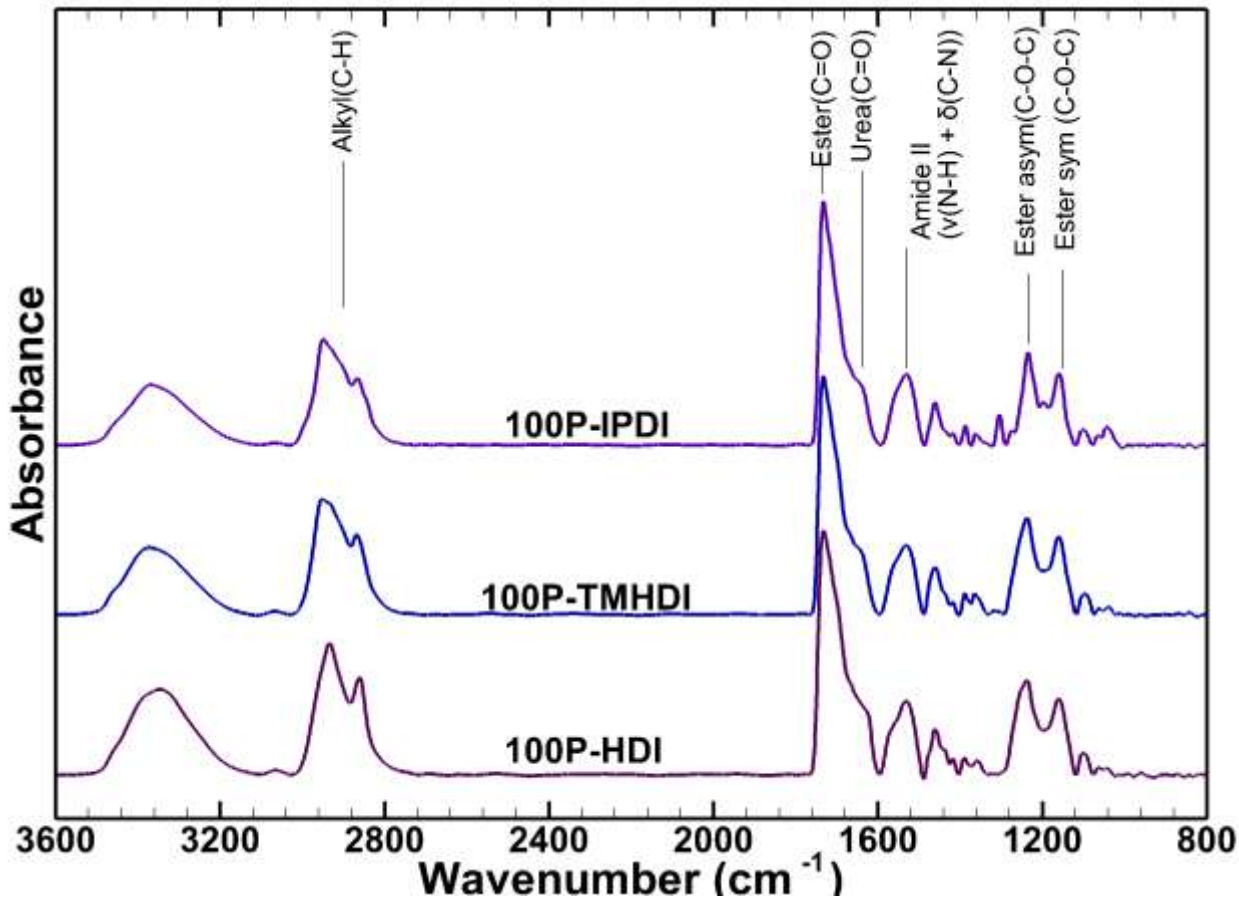

Figure 4. FTIR spectra of samples with the varying isocyanate type prior to degradation. Peaks corresponding to the alkyl, ester, urethane and urea bonds are labeled for identification.

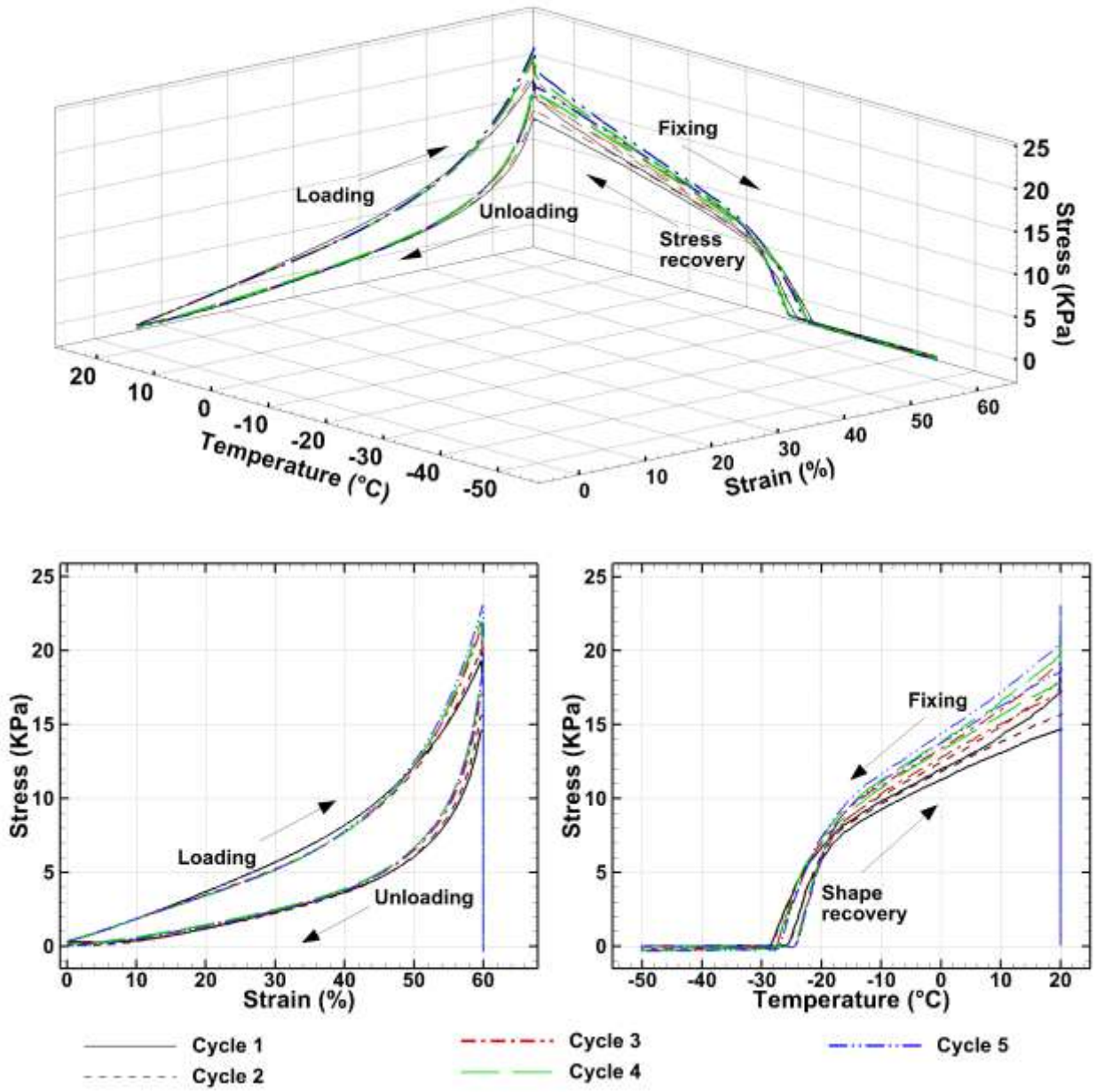

Figure 5. Constrained stress recovery shape memory tests of the 100P-HDI foam samples. The results for five cycles, representing the variation in sample stress with changes in strain and temperature during the loading, fixing, stress recovery and unloading steps, are shown in 3-D (top) and 2-D (bottom) formats.

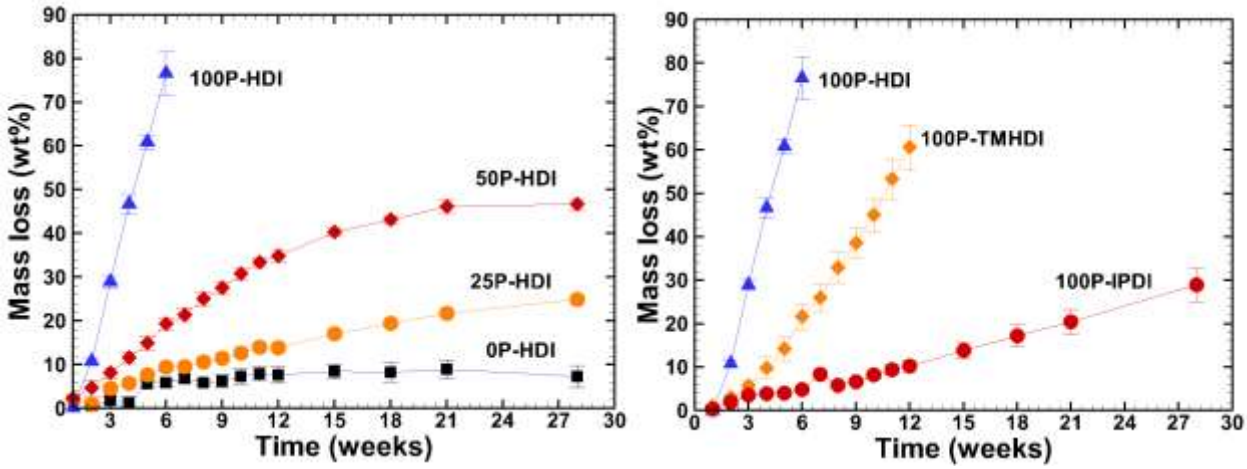

Figure 6. Mass loss profile of the different foam compositions over the first 28 weeks in 0.1 N NaOH media. The fastest mass loss is seen in the 100P-HDI composition, which has the highest PCL-t content and the most hydrophilic isocyanate monomer. The rate of mass loss is observed to decrease with both a decreasing PCL-t content, and increasing hydrophobicity of the isocyanate monomer.

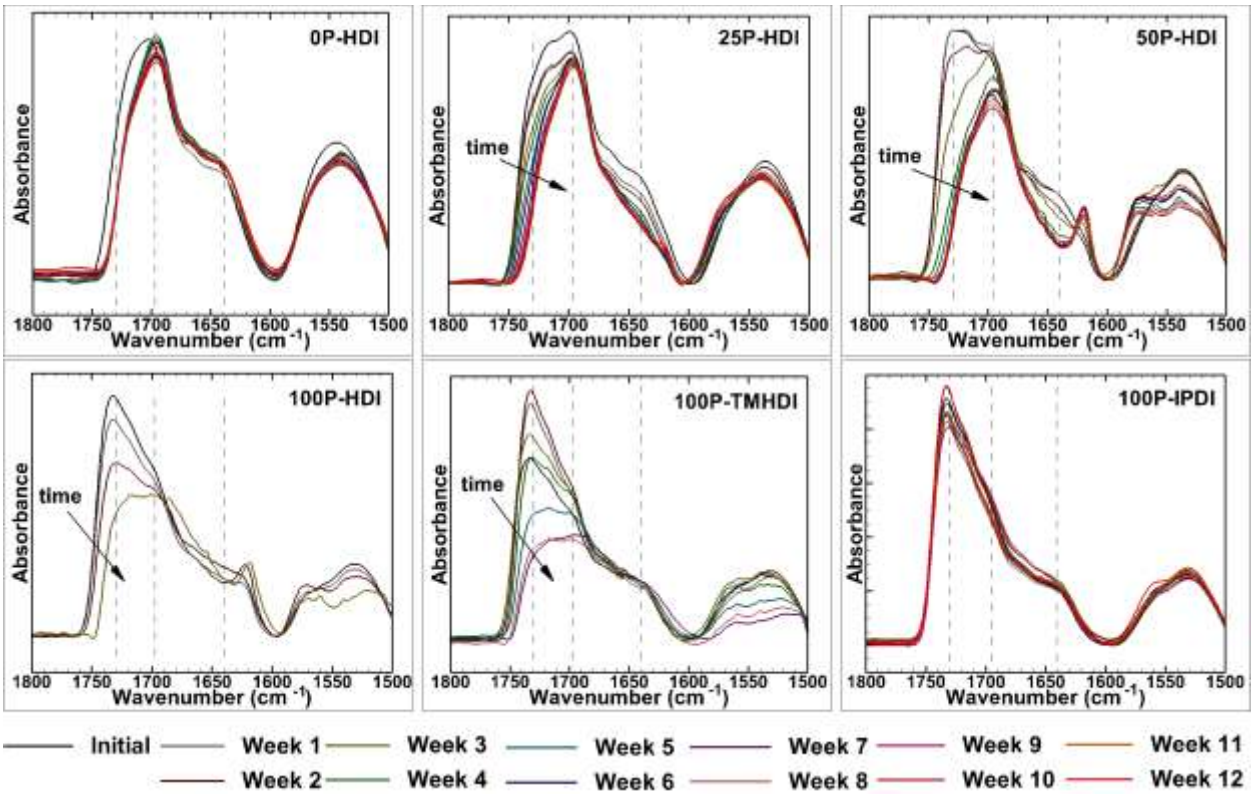

Figure 7. FTIR spectra for all the different compositions are shown as a function of time. The wavenumbers of interest, i.e. ester (1730 cm^{-1}), urethane (1695 cm^{-1}), and urea (1640 cm^{-1}) are marked with dotted lines.

Figure 8. Gross morphology of a 100P-HDI composition sample as it degraded over the first 6 weeks. Uniform degradation was observed to occur throughout the bulk of the material, leading to a continuous thinning of the sample, until it became irretrievable at week 7.

Table 1. Composition of different foams tested in the study. 0P-HDI, 25P-HDI, 50P-HDI and 100P-HDI denote an increasing concentration of the biodegradable monomer (PCL-t). 100P-TMHDI and 100P-IPDI denote substitution of HDI in the 100P-HDI composition with an equivalent amount of TMHDI and IPDI respectively.

Sample ID	HDI (wt.%)	TMHDI (wt.%)	IPDI (wt.%)	HPED (wt.%)	TEA (wt.%)	PCL-t (wt.%)	Water (wt.%)	DC5179 (wt.%)	DCI990 (wt.%)	T-131 (wt.%)	BL-22 (wt.%)
0P-HDI (Control)	62.85	-	-	19.68	6.68	0.00	2.76	3.82	3.31	0.26	0.64
25P-HDI	50.29	-	-	12.03	4.08	24.67	2.21	2.75	3.00	0.28	0.70
50P-HDI	42.19	-	-	6.73	2.28	41.39	1.85	1.91	2.55	0.31	0.79
100P-HDI	32.07	-	-	-	-	62.93	1.41	-	2.23	0.39	0.98
100P-TMHDI	-	37.12	-	-	-	58.25	1.30	-	2.06	0.36	0.90
100P-IPDI	-	-	38.42	-	-	57.04	1.28	-	2.02	0.35	0.89

Table 2. Average foam densities and glass transition temperatures for the different compositions.

Sample ID	Density (g cm^{-3})	T_g (°C)
0P-HDI (control)	0.020±0.002	70
25P-HDI	0.025±0.005	29
50P-HDI	0.047±0.015	11
100P-HDI	0.036±0.002	-19
100P-TMHDI	0.093±0.012	-11
100P-IPDI	0.035±0.005	26

8. References

[1] Brisman JL, Song JK, Newell DW. Cerebral aneurysms. New Engl J Med 2006;355:928-39.
[2] Zubillaga AF, Guglielmi G, Vi F, Duckwiler G. Endovascular occlusion of intracranial aneurysms with electrically detachable coils: correlation of aneurysm neck size and treatment results. Am J Neuroradiol 1994;15:815-20.
[3] Willinsky RA. Detachable coils to treat intracranial aneurysms. Can Med Assoc J 1999;161:1136-.
[4] Choudhari KA, Flynn PA, McKinstry SC. Spontaneous extrusion of guglielmi detachable coils from anterior communicating artery aneurysm. Neurol India 2007;55:148.
[5] Metcalfe A, Desfaits AC, Salazkin I, Yahia L, Sokolowski WM, Raymond J. Cold hibernated elastic memory foams for endovascular interventions. Biomaterials 2003;24:491-7.
[6] Maitland DJ, Small W, Ortega JM, Buckley PR, Rodriguez J, Hartman J, et al. Prototype laser-activated shape memory polymer foam device for embolic treatment of aneurysms. J Biomed Opt 2007;12:030504.
[7] Hayashi S, Fujimura H. Shape memory polymer foam. Mitsubishi Jukogyo Kabushiki Kaisha, Tokyo, Japan. U.S. Patent no. 5,049,591; 1991.
[8] Tobushi H, Okumura K, Endo M, Hayashi S. Thermomechanical Properties of Polyurethane-Shape Memory Polymer Foam. J Intel Mat Syst Str 2001;12:283-7.
[9] Tobushi H, Matsui R, Hayashi S, Shimada D. The influence of shape-holding conditions on shape recovery of polyurethane-shape memory polymer foams. Smart Mater Struct 2004;13:881.
[10] Di Prima M, Lesniewski M, Gall K, McDowell D, Sanderson T, Campbell D. Thermo-mechanical behavior of epoxy shape memory polymer foams. Smart Mater Struct 2007;16:2330.
[11] Domeier L, Nissen A, Goods S, Whinnery LR, McElhanon J. Thermomechanical characterization of thermoset urethane shape‐memory polymer foams. J Appl Polym Sci 2010;115:3217-29.
[12] De Nardo L, Bertoldi S, Tanzi M, Haugen H, Farè S. Shape memory polymer cellular solid design for medical applications. Smart Mater Struct 2011;20:035004.
[13] Hearon K, Singhal P, Horn J, Small W, Olsovsky C, Maitland KC, et al. Porous Shape Memory Polymers. Polymer Reviews 2012:(accepted).
[14] Singhal P, Rodriguez JN, Small W, Eagleston S, Van de Water J, Maitland DJ, et al. Ultra low density and highly crosslinked biocompatible shape memory polyurethane foams. J Polym Sci B Polym Phys 2012;50:724-37.
[15] Wilson T, Bearinger J, Herberg J, Marion III J, Wright W, Evans C, et al. Shape memory polymers based on uniform aliphatic urethane networks. J Appl Polym Sci 2007;106:540-51.
[16] Rodriguez JN, Yu YJ, Miller MW, Wilson TS, Hartman J, Clubb FJ, et al. Opacification of Shape Memory Polymer Foam Designed for Treatment of Intracranial Aneurysms. Ann Biomed Eng 2011:1-15.
[17] Hwang W, Volk B, Akberali F, Singhal P, Criscione J, Maitland D. Estimation of aneurysm wall stresses created by treatment with a shape memory polymer foam device. Biomech Model Mechanobiol 2012;11:715-29.
[18] Yu YJ, Hearon K, Wilson TS, Maitland DJ. The effect of moisture absorption on the physical properties of polyurethane shape memory polymer foams. Smart Mater Struct 2011;20:085010.
[19] Singhal P, Boyle T, Infanger S, Letts S, Small W, Maitland DJ, et al. Controlling the rate of actuation of shape memory polymer foams in water. Macromol Chem Phys 2012;(in press) DOI: 10.1002/macp.201200342.
[20] Rodriguez JN, Clubb F, Wilson TS, Miller MW, Fossum T, Hartman J, et al. In vivo tissue response following implantation of shape memory polyurethane foam in a porcine aneurysm model. J Biomed Mater Res Part A 2012:(submitted).

[21] Guarino V, Ambrosio L. The synergic effect of polylactide fiber and calcium phosphate particle reinforcement in poly ε-caprolactone-based composite scaffolds. Acta Biomater 2008;4:1778-87.
[22] Vaquette C, Kahn C, Frochot C, Nouvel C, Six JL, De Isla N, et al. Aligned poly(L-lactic-co-e-caprolactone) electrospun microfibers and knitted structure: a novel composite scaffold for ligament tissue engineering. J Biomed Mater Res A 2010;94:1270-82.
[23] Li W-J, Cooper Jr JA, Mauck RL, Tuan RS. Fabrication and characterization of six electrospun poly(α-hydroxy ester)-based fibrous scaffolds for tissue engineering applications. Acta Biomater 2006;2:377-85.
[24] Chen H, Huang J, Yu J, Liu S, Gu P. Electrospun chitosan-graft-poly (ε-caprolactone)/poly (ε-caprolactone) cationic nanofibrous mats as potential scaffolds for skin tissue engineering. Int J Biol Macromol 2011;48:13-9.
[25] Nisbet DR, Rodda AE, Horne MK, Forsythe JS, Finkelstein DI. Neurite infiltration and cellular response to electrospun polycaprolactone scaffolds implanted into the brain. Biomaterials 2009;30:4573-80.
[26] Liu JJ, Wang CY, Wang JG, Ruan HJ, Fan CY. Peripheral nerve regeneration using composite poly(lactic acid-caprolactone)/nerve growth factor conduits prepared by coaxial electrospinning. J Biomed Mater Res A 2011;96:13-20.
[27] Heydarkhan-Hagvall S, Schenke-Layland K, Dhanasopon AP, Rofail F, Smith H, Wu BM, et al. Three-dimensional electrospun ECM-based hybrid scaffolds for cardiovascular tissue engineering. Biomaterials 2008;29:2907-14.
[28] Ulery BD, Nair LS, Laurencin CT. Biomedical applications of biodegradable polymers. J Polym Sci B Polym Phys 2011;49:832-64.
[29] David D, Silverstein MS. Porous polyurethanes synthesized within high internal phase emulsions. J Polym Sci A Polym Chem 2009;47:5806-14.
[30] Socrates G. Infrared Characteristic Group Frequencies: Tables and Charts. NewYork: Wiley & Sons; 1994.
[31] Behl M, Zotzmann J, Schroeter M, Lendlein A. Biodegradable Shape Memory Polymers. In: Lendlein A, Sisson A, editors. Handbook of Biodegradable Polymers: Synthesis, Characterization and Applications. First ed: Wiley-VCH Verlag GmbH & Co.; 2011.
[32] Alteheld A, Feng Y, Kelch S, Lendlein A. Biodegradable, amorphous copolyester‐urethane networks having shape‐memory properties. Angew Chem Int Edit 2005;44:1188-92.
[33] Choi N-y, Lendlein A. Degradable shape-memory polymer networks from oligo[(l-lactide)-ran-glycolide]dimethacrylates. Soft Matter 2007;3:901-9.
[34] Choi NY, Kelch S, Lendlein A. Synthesis, Shape‐Memory Functionality and Hydrolytical Degradation Studies on Polymer Networks from Poly (rac‐lactide)‐b‐poly (propylene oxide)‐b‐poly (rac‐lactide) dimethacrylates. Adv Eng Mater 2006;8:439-45.
[35] Göpferich A. Mechanisms of polymer degradation and erosion. Biomaterials 1996;17:103-14.